http://dx.doi.org/10.11142/jicems.2014.3.1.32

Modelling and Optimal Design of a Ring-type Structure for the Generation of a Traveling Wave

Xinchang Liu *, Yoan Civet *, and Yves Perriard *

Abstract – Traveling wave generation in a ring type stator has been studied. The basic working principle to create traveling wave has been modelled by the superposition of two orthogonal standing waves. Theoretical analysis shows that the length to radius ratio affects the frequency gap between two pseudo orthogonal modes used to create traveling wave. FEM simulation is then discussed and applied to validate the analytical model. At last, a possible optimal solution is reported with FEM verification.

Keywords: Ring-type motor, Ultrasonic motor, Traveling wave, Piezoelectric

1. Introduction

Over the past few decades, traveling wave piezoelectric motor, also called piezoelectric ultrasonic motor, has been widely investigated because of its advantages for low speed, high torque and compact applications. Divers types of traveling wave piezoelectric motor have been studied [1], especially, rotary motor has attracted most attentions. Detailed analytical model using classical approach such as Hamilton's principle [2], [3] could demonstrate the mechanism of operating principle and help the design of the motor.

Similar to traveling wave rotary motor, a traveling wave piezoelectric linear motor uses friction force to create linear movement between a slider and a beam. Kuribayashi et Al. [4] built the first prototype in 1985 with a vibrator-absorber system. Several other articles reported the application of linear traveling wave motor based on the same principle of rotary traveling wave motor by superposing orthogonal standing waves [5], [6]. But the edge reflexion is still a problem and damping material is needed at the boundaries to prevent from the reflection [7].

In order to reduce the effect of reflection, a ring type structure, which consists of two straight parts and two curved parts, could guide the wave to travel along it and thus avoid reflection. This idea was firstly mentioned in literature in 1990 [8], then the first prototype was reported 6 years later by Seemann et Al. [9]. The principle to create traveling wave is the same as the one of traveling wave rotary motor. However, a ring type stator does not have infinite helical symmetry as the stator of a rotary motor, hence, the resonant frequencies of two orthogonal modes have normally a difference between them [10]. Seemann et Al. [9] reported a numerical method to find the frequency intersections of two orthogonal modes. The ratio between the length of straight part and the radius of curved part has been studied in order to find the coincide resonant frequencies.

Previous works about ring-type motor are mainly based on Finite Element Method (FEM). Numerical results could be useful for a specific configuration but limited to explain intrinsic relations in a general ring type structure. Therefore, this paper focuses on the modelling and optimal design of the ring type structure with the purpose of creating a continuous stable traveling wave. The first part will introduce the principle of operation of a traveling wave motor. A detailed analytical model will be presented in the following part. Then, simulation and comparison with analytical results will be given and an optimal design will be proposed at the end.

2. Stator geometry and operation principle

A ring type stator is characterised by two straight parts of length L and two semicircles of radius R for the middle plan as shown in Fig.1. The thickness is h with the hypothesis that $h \ll L$. Note that the width is w, thus, the cross section A of the structure is $A = wh$. In the following study, the length to radius ratio $\eta = \frac{L}{R}$ will also be used to represent the structure configuration. Due to the symmetry of the

* Institut of Microengineering (IMT), Integrated Actuators Laboratory (LAI), École Polytechnique Fédérale de Lausanne (EPFL), Switzerland.(xinchang.liu@epfl.ch,yoan.civet@epfl.ch, yves.perriard@epfl.ch)
Received 21 October 2013; Accepted 28 November 2013

structure, we will only consider the top straight part and the right curved part in the following analysis.

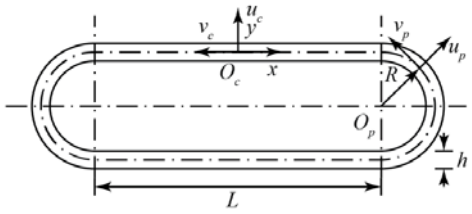

Fig. 1. A ring type structure

Classical principle of traveling wave motor uses superposition of two standing waves with same amplitude, same angular frequency, same wavelength and 90º phase shift both in space and temporal domains. The well-known trigonometric equation of vertical movement of the middle plan $u_c(x,t)$ in the straight part is:

$$\begin{aligned} u_c(x,t) &= C\cos(\omega t)\cos(kx) + C\sin(\omega t)\sin(kx) \\ &= C\cos(\omega t - kx) \end{aligned} \tag{1}$$

where ω stands for the angular frequency and k is the wave number.

With the vertical movement of the middle line described in (1), the structure is bended periodically and the points of surface follow an elliptical motion [2]. A movable "rotor" is placed on it. The wave crests act as the contact points between rotor and stator. Due to the elliptical motion, the contact points have a velocity parallel to the axis x. Relative movement between rotor and contact points leads to a frictional force along axis x, thus, a movement in the same direction. To ensure the driving effect, a stable traveling wave on the structure is the key point for success.

3. Stator modelling

The straight part and the curved part of stator could be analysed separately with respect of coherent boundary conditions. Based on bending theory and linear theory of elasticity, differential equations could be established at first time. The solutions under consideration of coupled frequency could then describe the vibratory motion of the structure. The objective of the modelling is to prove that it is possible to obtain a pair of sinusoidal waves in the structure for each mode and thus to obtain a traveling wave using their superposition. The mathematical result should also forecast the wave parameters, such as wavelength and resonance frequency.

3.1 Straight part

Let's assume $O_c(x, y)$ being the Cartesian coordinate system with the origin at geometric centre of the top straight part as shown in Fig.1. Applying the Euler-Bernoulli beam theory, we can find related equations of a vibratory beam [11]. The deformation energy V and the kinetic energy T can be written as:

$$\mathcal{V}_{c,u} = \frac{1}{2}\int_{-\frac{L}{2}}^{\frac{L}{2}} -EI_h\left(\frac{\partial^2 u_c}{\partial x^2}\right)^2 dx \tag{2}$$

$$\mathcal{T}_{c,u} = \frac{1}{2}\int_{-\frac{L}{2}}^{\frac{L}{2}} \rho A\left(\frac{\partial u_c}{\partial t}\right)^2 dx \tag{3}$$

where I_h is second moment of area and E is young's modulus.

Considering the horizontal motion of the beam v_c, from Hooke's law and linear elastic theory we have:

$$\mathcal{V}_{c,v} = \frac{1}{2}\int_{-\frac{L}{2}}^{\frac{L}{2}} -EA\left(\frac{\partial v_c}{\partial x}\right)^2 dx \tag{4}$$

$$\mathcal{T}_{c,v} = \frac{1}{2}\int_{-\frac{L}{2}}^{\frac{L}{2}} \rho A\left(\frac{\partial v_c}{\partial t}\right)^2 dx \tag{5}$$

The hypothesis $h \ll L$ supposes that the variation of h caused by v_c is also very small compared to u_c, so that h is considered as constant in the following steps.

By using the Euler-Lagrange equation

$$\mathcal{L}_c = \mathcal{T}_{c,u} + \mathcal{T}_{c,v} - \mathcal{V}_{c,u} - \mathcal{V}_{c,v} \tag{6}$$

Taking (2), (3), (4) and (5) into (6) and applying the Hamilton's principle for variables uc and vc. We can obtain the following equation:

$$\frac{\partial \mathcal{L}_c}{\partial u_c} - \frac{\partial}{\partial t}\frac{\partial \mathcal{L}_c}{\partial u_{c,t}} + \frac{\partial}{\partial x^2}\frac{\partial \mathcal{L}_c}{\partial u_{c,xx}} = -\rho A\frac{\partial^2 u_c}{\partial t^2} - EI_h\frac{\partial^4 u_c}{\partial x^4} = 0 \tag{7}$$

and the equation of perpendicular movement is

$$\frac{\partial \mathcal{L}_c}{\partial v_c} - \frac{\partial}{\partial t}\frac{\partial \mathcal{L}_c}{\partial v_{c,t}} - \frac{\partial}{\partial x}\frac{\partial \mathcal{L}}{\partial v_{c,x}} = -\rho A\frac{\partial^2 v_c}{\partial t^2} + EA\frac{\partial^2 v_c}{\partial x^2} = 0 \tag{8}$$

3.2 Curved part

Let's assume Op(θ, r) being the polar coordinate system in which the pole coincides with the centre of the semicircle. Firstly, assuming at the middle line of the semi-circle, we have:

$$\frac{d\theta}{ds} = \frac{1}{R} \tag{9}$$

where *s* is the middle line arc length of curved part. If we consider a small variation of middle line, we have:

$$\frac{d\theta + \Delta d\theta}{ds + \Delta ds} = \frac{1}{R'} \tag{10}$$

The bending force in the material of a curved beam can then be calculated thanks to the variation of radius of curvature [12]:

$$\frac{1}{R'} - \frac{1}{R} = -\frac{M}{EI_h} = \frac{d^2u_p}{ds^2} + \frac{u_p}{R^2} \tag{11}$$

Then, taking into account (9), the expression of vibrational potential energy of the curved part Vp can be obtained:

$$\mathcal{V}_p = \frac{1}{2}\int_{-\frac{\pi}{2}}^{\frac{\pi}{2}} \frac{EI_h}{R^3}\left(\frac{\partial^2 u_p}{\partial\theta^2} + u_p\right)^2 d\theta \tag{12}$$

Identical to the straight part, the kinetic energy Tp is of the following form:

$$\mathcal{T}_p = \frac{1}{2}\int_{-\frac{\pi}{2}}^{\frac{\pi}{2}} \rho A\left(\left(\frac{\partial u_p}{\partial t}\right)^2 + \left(\frac{\partial v_p}{\partial t}\right)^2\right) d\theta \tag{13}$$

Notice that the curved part is a semi-circle, the relation between normal movement and tangent movement is $u_p = \frac{\partial v_p}{\partial \theta}$. Therefore, using (13) and applying the Hamilton's principle, we have

$$\begin{aligned}\mathcal{L}_p &= \mathcal{T}_p - \mathcal{V}_p \\ &= \frac{1}{2}\int_{-\frac{\pi}{2}}^{\frac{\pi}{2}} \frac{EI_h}{R^3}\left(\frac{\partial^3 v_p}{\partial\theta^3} + \frac{\partial v_p}{\partial\theta}\right)^2 d\theta \\ &\quad - \frac{1}{2}\int_{-\frac{\pi}{2}}^{\frac{\pi}{2}} \rho AR\left(\left(\frac{\partial}{\partial t}\frac{\partial v_p}{\partial\theta}\right)^2 + \left(\frac{\partial v_p}{\partial t}\right)^2\right) d\theta\end{aligned} \tag{14}$$

Lp is a function of v(t, θ) with up to third order derivative. In (15), zero terms are ignored.

$$\frac{\partial\mathcal{L}_p}{\partial v_p} - \frac{\partial}{\partial t}\frac{\partial\mathcal{L}_p}{\partial v_{p,t}} - \frac{\partial}{\partial\theta}\frac{\partial\mathcal{L}_p}{\partial v_{p,\theta}} + \frac{\partial^2}{\partial t\partial\theta}\frac{\partial\mathcal{L}_p}{\partial v_{p,t,\theta}} - \frac{\partial^3}{\partial\theta^3}\frac{\partial\mathcal{L}_p}{\partial v_{p,\theta^{(3)}}} = 0 \tag{15}$$

Replacing Lp from (14) in (15):

$$\begin{aligned}&\rho AR\left(\frac{\partial^2 v_p}{\partial t^2} - \frac{\partial^2}{\partial t^2}\frac{\partial^2 v_p}{\partial\theta}\right) \\ &\quad - \frac{EI_h}{R^3}\left(\frac{\partial^6 v_p}{\partial\theta^6} + 2\frac{\partial^4 v_p}{\partial\theta^4} + \frac{\partial^2 v_p}{\partial\theta^2}\right) = 0\end{aligned} \tag{16}$$

Equations (7), (8) and (16) form a system of equations which describes the movement of the ring type structure.

3.3 Boundary conditions

Because of the continuity of the structure, at $O_c(\frac{L}{2}, y)$ and $O_p(\frac{\pi}{2}, R)$, the two sections have the same movement. Thus, on the middle line of these section, they have same displacement and same derivative with respect to x or θ. The boundary conditions can then be written as follows:

$$u_c\left(\frac{L}{2}, t\right) = u_p\left(\frac{\pi}{2}, t\right) \tag{17}$$

$$\frac{du_c(\frac{L}{2}, t)}{dx} = \frac{du_p(\frac{\pi}{2}, t)}{dx} \tag{18}$$

At the intersection of the two coordinate systems, we have *dx* = -*ds*. On the right side of (18), du_p is a function of θ. Equation (18) can be rewritten as:

$$\frac{du_c(\frac{L}{2}, t)}{dx} = -\frac{du_p(\frac{\pi}{2}, t)}{Rd\theta} \tag{19}$$

3.4 Equations and properties

From (7), (8) and (16), we can verify that the solution can be a sinusoidal function of time with a time independent coefficient.

$$u(\alpha, t) = U(\alpha)\sin(\omega t + \varphi) \tag{20}$$

where α stands for *x* or θ.

Equations (7), (8) and (16) become

$$u_{c,x^{(4)}} - \left(\frac{\omega_{u_c}}{a}\right)^2 u_{c,x} = 0 \tag{21}$$

$$v_{c,x^{(2)}} - \left(\frac{\omega_{v_c}}{b}\right)^2 v_{c,x} = 0 \tag{22}$$

$$u_{p,\theta^{(6)}} + 2u_{p,\theta^{(4)}} + u_{p,\theta^{(2)}} - \left(\frac{\omega_{u_p}R^2}{a}\right)^2 (u_{p,\theta^{(2)}} - u_{p,\theta}) = 0 \tag{23}$$

with $a = \sqrt{\frac{EI_h}{\rho A}}$, $b = \sqrt{\frac{E}{\rho}}$. $u_{c,\alpha^{(i)}}$ stands for the i^{th} order partial derivative of u_c with respect to the variable α.

The resonance frequency of the whole structure depends on the eigen frequencies of each part. Maximum amplitude can be found while their frequencies are coupled in function of the material itself and geometric parameters a and b.

The solution of above differential equations is of the form

$$U(s) = A_1\cos(k_s s) + A_2\sin(k_s s) + A_3\cosh(k_s s) + A_4\sinh(k_s s) \quad (24)$$

We will prove that the particular solutions could only be in form of cos or sin for a ring type structure. As the general solution is the sum of an even function and an odd function, let's assume firstly it exists an even solution for the straight part, so we have $u_c\left(-\frac{L}{2}\right) = u_c\left(\frac{L}{2}\right)$. From (17), at the upper end of curved part, $u_p\left(\frac{\pi}{2}\right) = u_c\left(\frac{L}{2}\right)$. And at the other end, taking into account the symmetry of structure geometry, there are two possibilities: mirror symmetry with the perpendicular axis and origin symmetry with the central of the structure. Hence, in case of mirror symmetry, $u_p\left(-\frac{\pi}{2}\right)$ is equal to $-u_p\left(\frac{\pi}{2}\right)$ which corresponds to a solution of odd function for the curved part; otherwise, $u_p\left(-\frac{L}{2}\right)$ is equal to $-u_c\left(\frac{L}{2}\right)$ and it results an even solution for the semicircle. Secondly, if a solution contains cosh or sinh, it is not possible to find a solution with the form of (24) which meets the continuity condition (19). As a result, the particular solutions of the ring type structure are the eight non-repetitive combination pairs of ±sin or ±cos functions for straight and curved part. We can then note for example $\{A_{u,c}\cos(k_{u,c}x)$, $-A_{u,p}\cos(k_{u,p}\theta)\}$ as the form of one possible particular solution of the problem.

Considering the coupling of vertical movement of the structure, it can be supposed that the vertical vibration frequency should be the same, thus, $\omega_{u,c} = \omega_{u,p}$. Knowing the resonance frequency equations (21), (23) and boundary conditions (11), (19), we can take one possible form of particular solutions, such as $A_{u,c}\cos(k_{u,c}x)$ for straight part and $A_{u,p}\cos(k_{u,p}\theta)\}$ for curved part. Then, we have

$$ak_{u_c}^2 = \frac{a}{R^2}\sqrt{\frac{k_{u_p}^6 - 2k_{u_p}^4 + k_{u_p}^2}{1 + k_{u_p}^2}} \quad (25)$$

$$A_{u_c}\cos(k_{u_c}\frac{L}{2}) = A_{u_p}\cos(k_{u_p}\frac{\pi}{2}) \quad (26)$$

$$A_{u_c}k_{u_c}\sin(k_{u_c}\frac{L}{2}) = -\frac{A_{u_p}k_{u_p}}{R}\sin(k_{u_p}\frac{\pi}{2}) \quad (27)$$

Simplifying (25), we will directly have the relation between ku,c and ku,p

$$k_{u_c}^2R^2 = (k_{u_p}^2 - 1)\sqrt{\frac{k_{u_p}^2}{1 + k_{u_p}^2}} \quad (28)$$

which shows that ku,p should be bigger than one and always bigger than ku,cR. Physically, it means that the wavelength on the curved part is always smaller than the wavelength from the straight part. And the wavelength from the curved part could not be less than the circumference of it. Also from (28), as the wave number increases, the wavelength will approach to the value of straight part. These results imply that because of the intersection, wave velocity will be changed.

Introducing the ratio between the amplitude of two parts $\gamma = \frac{A_{up}}{A_{uc}}$, an intermediate variables $k_0 = \frac{k_{up}^2}{1+k_{up}^2}$ and replacing $k_{u,c}$ in (26) and (27) using (28), we have

$$\cos^2(k_{u_c}\frac{L}{2}) = \frac{(\gamma^2 - k_0)k_{u_p}^2 + k_0}{(1 - k_0)k_{u_p}^2 + k_0} \quad (29)$$

It is necessary that (29) has at least a valid solution and it can be deduced that γ should be smaller than 1, whose physic meaning is that the amplitude on the curved part is always smaller than that on the straight part.

3.5 Solutions

Given the length and the radius of the structure, it is wanted to have the value of ku,c and ku,p. However, transcendental equations do not allow analytical solution. Therefore, a numerical approach is applied to solve these equations.

Expressing γ in three ways respectively from (26), (27) and (29):

$$\gamma_1 = \frac{\cos(k_{u_c}\frac{L}{2})}{\cos(k_{u_p}\frac{\pi}{2})} \quad (30)$$

$$\gamma_2 = \frac{\sin(k_{u_c}R\frac{L}{2})}{k_{u_p}\sin(k_{u_p}\frac{\pi}{2})} \quad (31)$$

$$\gamma_3 = \sqrt{\frac{\cos^2(k_{u_c}\frac{L}{2})((1 - k_0)k_{u_p}^2 + k_0)}{k_{u_p}^2} + k_0} \quad (32)$$

From (28), ku,c can be explicitly expressed by ku,p. The problem of solving a system of transcendental equations can be turned to the following problem with a single variable ku,p.

$$f(k_{u_p}) = (\gamma_1 - \gamma_2)^2 + (\gamma_2 - \gamma_3)^2 + (\gamma_3 - \gamma_1)^2 = 0 \quad (33)$$

The solutions will be obtained only if the condition γ1 = γ2 = γ3 = γ is satisfied. Using the propriety that 0 < γ < 1, it only needs to search the range where f is smaller than 3. Furthermore, a solution must be a local minimum of f, thus, efficient numerical method can be applied to find the approximated solutions of ku,p.

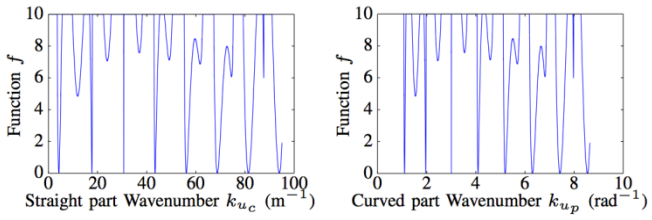

(a) $f(k_{u_c})$ (b) $f(k_{u_p})$

Fig. 2. Function f with given L = 0.717 m and R = 0.09 m for the particular solution form{$A_{u,c}\cos(k_{u,c}x)$, -$A_{u,p}\cos(k_{u,p}\theta)$}

With $k_{u,p}$ solved in previous step, $k_{u,c}$ can be deduced by (28) and then the related angular resonance frequency from (21) can be expressed as

$$\omega = 2\pi f = ak_{u_c}^2 \tag{34}$$

Similar approach could also be applied for the horizontal movement on the straight part. From (22) and (23), by coupling the resonance frequency, we can also obtain a system of equations whose solutions correspond to the wavelength of horizontal vibration modes.

3.6 Scaling factor

If the length to radius ratio is fixed, when the geometric configuration of ring type structure changes, the solutions of vibration modes are still valid by multiplying by a scaling factor. Let's suppose the structure is scaled p times. The geometric parameters of the new structure are $L' = pL$, $R'=pR$, $h' = ph$. Then, taking $k'_{u,c} = \frac{k_{u,c}}{p}$ and $k'_{u,p} = k_{u,p}$ into (25), (26) and (27), the same equations are obtained. Thus, $k'_{u_c} = \frac{k_{u_c}}{p}$ is the solution for the scaled structure.

From (34), the resonance frequency will become

$$\omega'_{u_c} = a'k'^2_{u_c} = \sqrt{\frac{E}{12\rho}}h'k'^2_{u_c} = \frac{\omega_{u_c}}{p} \tag{35}$$

If only the thickness is scaled q times and the other parameters do not change, $k_{u,c}$ stays identical to $k'_{u,c}$ and we have

$$\omega'_{u_c} = q\omega_{u_c} \tag{36}$$

We can introduce a level set $S(C) = \{(L, R)|L + \pi R - C = 0\}$ where C is a constant. As C and $\eta = \frac{L}{R}$ are sufficient to define a unique pair of configuration (L, R), it is possible to study the structure with these two parameters η and C. With scaling properties, if $k_{uc}(\eta, C)$ is a solution of a certain configuration, for another configuration of the same length to radius ratio but a different C, we have $\frac{k'_{u,c}(\eta,C')}{k_{u,c}(\eta,C)} = \frac{C}{C'}$. Therefore, we can firstly choose a C and change the value of η. The results obtained can then be applied to other C thanks to the scaling property.

Given (η, C), from (36), the resonance frequency is linear according to the thickness. In order to study the influence of h, it is also possible to scale the frequencies to an equivalent frequency for different h. Thus, we can compare the results.

3.7 Pseudo orthogonal modes

Considering two of the eight combinations of particular solutions, such as {$A_{u,c}\cos(k_{u,c}x)$, -$A_{u,p}\cos(k_{u,p}\theta)$} and {$A'_{u,c}\sin(k_{u,c}x)$, -$A'_{u,p}\sin(k'_{u,p}\theta)$}, we can solve $k_{u,c}$ and $k'_{u,c}$ respectively with the condition that C = 1 m.

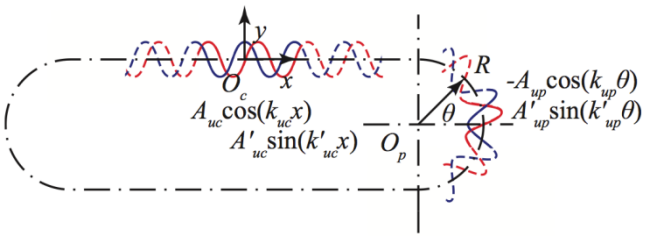

Fig. 3. Two solution forms for the middle line

In Fig. 3, for both solutions, it can be noticed that from O_c(0,0) to O_p(0,R) there should be n + 0.5 periods. Due to the symmetry, the results of these two solutions are related to the 4n + 2 modes. Moreover, the wavelength depends on $k_{u,c}$ and $k'_{u,c}$. If they share the same value, the two modes become orthogonal to each other. We can then plot $k_{u,c}$ and $k'_{u,c}$ in function of η.

As shown in Fig. 2a, with a given geometric configuration, $f(k_{u,c})$ has multiple solutions and each solution corresponds to one n related to the mode order. We can take for example the second solution (around 20 m^{-1}) to illustrate the results. The related n is 1 and 4n + 2 = 6, thus, it is the 6th mode.

Fig. 4 shows the variation of $k_{u,c}$ and $k'_{u,c}$ for the 6th mode. It can be noticed that the two modes do not always have the same k, but they are very close to each other and have three intersections in total. As a result, we can call them pseudo orthogonal modes and only at the intersections, they become orthogonal.

In order to create a stable traveling wave, it is necessary to have two pseudo orthogonal modes with resonance frequencies (depend on k) as close as possible. We could play with the ratio η to find optimal design of the structure.

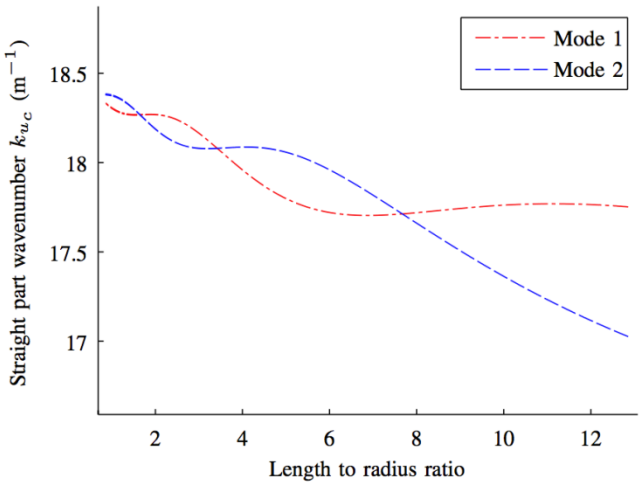

Fig. 4. Solution of two pseudo orthogonal modes (6th)

4. Simulation results

Simulations have been carried out under Comsol. The structure is supposed to be made of aluminium with the density ρ = 2.73 × 10^3 kg/m^3, young's modulus E = 6.9 × 10^{10} Pa and constant C = 200 mm. By varying the length to radius ratio and the thickness, eigenfrequency solutions can be obtained and the 6th mode is chosen as an example to compare with the theoretical results.

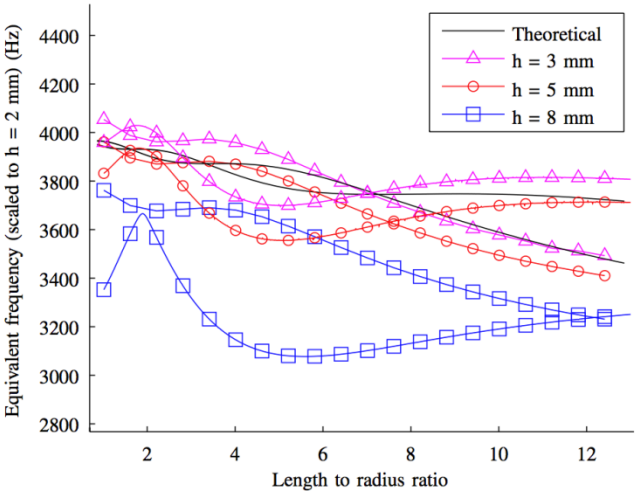

Fig. 5. Theoretical result of pseudo orthogonal modes and simulation results for various h

Fig. 5 shows the results of simulations. Due to variation of thickness, equivalent frequencies are used to facilitate the analysis of the data. The thickness of h = 2 mm is chosen as a reference configuration. Then, the results can be scaled using scaling factor introduced in the Section 3.6. The black curves stand for the theoretical solutions of pseudo orthogonal modes identical to Fig. 4; the other solutions marked with symbols are obtained by simulations for various thicknesses of 3 mm, 5 mm and 8 mm. Each result contains two lines and they correspond to the related pseudo modes. We can see the results with circle/triangle have three intersections between two pseudo orthogonal modes. They are coherent to the theoretical result.

Table 1. Simulation results of 6th modes for different thicknesses with equivalent frequency (C = 200 mm, h = 2 mm)

	Frequency (Hz)	Δf%	η	$\Delta\eta$%
Theoretical	3746	-	7.25	-
h = 2 mm	3786	1.1%	6.92	4.5%
h = 3 mm	3749	0.1%	7.02	3.1%
h = 4 mm	3698	1.3%	7.20	0.7%
h = 5 mm	3630	3.1%	7.50	3.5%
h = 6 mm	3542	5.5%	8.06	11.2%
h = 7 mm	3421	8.7%	9.16	26.3%
h = 8 mm	3238	13.6%	12.18	68.0%

Detailed results of third intersection are given in Table 1. For practical reason, only entire values of thickness are studied. As shown in Fig. 5, the thickness bigger than 6 mm will introduce an important relative error. While the length to radius ratio is small, the thickest structures (Square symbols at η = 2 lost frequency intersection of two pseudo orthogonal modes. This comes from previous hypothesis $h \ll L$ or $h \ll \lambda$, where λ is the wavelength of straight part. As the thickness becomes bigger, complex interaction inside the structure will be difficult to approximate by a linear model.

5. Optimal design

The goal of the study is to design the structure in an optimal way by using as much information as possible with the consideration of all constraints.

In our application, a beam of 160 mm is given as requirements. The other dimensions are not strictly constrained but we still do not target a huge system.

Step 1: Man should decide the length to radius ratio. For the low frequency application, theoretical analysis will be useful: it can help to choose a favourite ratio regarding to the constraints. For example, we prefer a ratio a little higher to save vertical space. But from previous analysis, it is demonstrated that if the circumference of curved part is less than the wavelength, there is no solution. So we cannot expect a very big ratio unless quite high frequency is acceptable. We can then concentrate on a reasonable ratio

around 7.

Step 2: A thickness could be taken by comparing the stability of the frequency and the intersection of two pseudo orthogonal modes. The Table 2 shows a possible solution not very sensitive to the change of thickness below 5 mm. But there is no intersection of two modes while the thickness is greater than 6 mm. We prefer a thicker structure in order to get a more important horizontal movement on the top surface. So we can choose η = 7.7 and h = 5 mm, while the constant C = 200 mm.

Table 2. Simulation results of 7th modes with equivalent frequency (C = 200 mm, h = 2 mm)

	Frequency (Hz)	$\Delta f\%$	η	$\Delta\eta\%$
Theoretical	5166	-	9.1	-
h = 2 mm	5298	2.6%	7.86	13.6%
h = 3 mm	5241	1.4%	7.84	13.8%
h = 4 mm	5165	0.2%	7.80	14.3%
h = 5 mm	5068	1.9%	7.67	15.8%
h = 6 mm	-	-	-	-

Step 3: we can calculate the configuration based on the parameters determined. The length of the straight part is 160 mm as the requirement. Then the radius $R = \frac{\eta}{L} \approx$ 20 mm. With h = 5 mm and using scaling factor, the estimated resonance frequency is 10257 Hz.

Step 4: knowing all the structure parameters, we can estimate the right placement of actuators. Due to the symmetry, one actuator could be directly placed at the centre of the bottom straight part. The other one could be placed nearby with a distance of 0.25λ. By solving the equation with current configuration, $k_{u,c}$ = 94.24 m^{-1}, so the wavelength $\lambda = \frac{2\pi}{k_{u,c}} =$ 66.7 mm. Thus, the distance for the placement of second piezo is 17 mm. If more actuators are required, this value can also be used to repeat the placement.

Step 5: the complete ring-type stator design is obtained. Under Comsol, this configuration can be verified by FEM method.

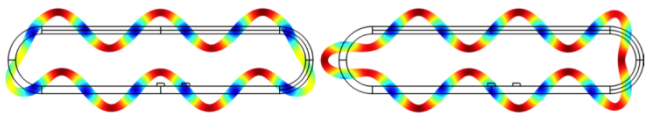

(a) Excitation result: mode 1 (b) Excitation result: mode 2

Fig. 6. Frequency domain simulation with piezoelectric actuator excitation at pseudo resonance frequency (f = 10300 Hz)

It can be observed in Fig. 6 two orthogonal modes. In fact, as result of approximation value used in the calculation regarding to the realistic constraints, the resonant frequencies of the two pseudo orthogonal modes are respectively 10259 Hz and 10320 Hz. But with a force vibration, we can still superpose the two frequencies as show in Fig. 6.

5. Conclusion

This article concentrates on the modelling of the ring type stator. Theoretical analysis using Hamilton's principle helps to obtain the differential equations which describe the vibrational movement of the structure. The transcendental equations of the problem have been transformed to single function depending only on the curved part wavenumber. Hence, once the structure's length and radio are known, we can obtain analytically the related wavenumber, wavelength and resonance frequency.

According to the scaling property, a normalised structure can serve as a standard configuration. Its result is then applied to other configurations using scaling factor. Given a constant C, pseudo orthogonal modes can be observed by varying the length to radius ratio, which explains the problematic of ring type stator: mechanical design is critical for the generation of traveling wave.

FE Simulations show the validation of the modelling, although a thicker structure results to failure of creating identical frequency modes. Unfortunately, the analytical model is no longer applicable in this case.

An optimal design of ring type stator is proposed at the end. With the 7th mode, we find that the variation of length to radius ratio becomes more stable at the intersection of pseudo modes. Finally, a structure 160 mm long, 4 mm thick and with a radius of 20 mm has been chosen as the final design. Two orthogonal modes are verified by simulation. The parameters and the behaviour are the same as predicted by the theoretical analysis. Our model is thus useful for design and optimisation.

References

[1] J. Fernandez and Y. Perriard, “Characteristics, modeling and simulation of a traveling wave ultrasonic linear motor,” in Ultrasonics Symposium, 2004 IEEE, vol. 3. IEEE, 2004, pp. 2247–2250.

[2] N. W. Hagood IV and A. J. McFarland, “Modeling of a piezoelectric rotary ultrasonic motor,” Ultrasonics, Ferroelectrics and Frequency Control, IEEE Transactions on, vol. 42, no. 2, pp. 210–224, 1995.

[3] N. El ghosty, “Hybrid modeling of a traveling wave piezoelectric motor,” Ph.D. dissertation, Aalborg University, 2000.

[4] M. Kuribayashi, S. Ueha, and E. Mori, “Excitation conditions of flexural traveling waves for a reversible ultrasonic linear motor,” The Journal of the Acoustical Society of America, vol. 77, p. 1431, 1985.
[5] P. Suybangdum, P. Smithmaitrie, and P. Laoratanakul, “Dual piezoelectic actuators for the traveling wave ultrasonic linear motor,” in Fourth International Conference on Experimental Mechanics. International Society for Optics and Photonics, 2009, pp. 75 223I–75 223I.
[6] Y. Roh, S. Lee, and W. Han, “Design and fabrication of a new traveling wave-type ultrasonic linear motor,” Sensors and Actuators A: Physical, vol. 94, no. 3, pp. 205–210, 2001.
[7] B. Dehez, C. Vloebergh, and F. Labrique, “Study and optimization of traveling wave generation in finite-length beams,” Mathematics and Computers in Simulation, vol. 81, no. 2, pp. 290–301, 2010.
[8] R. J. Zemella, “Design and development of a linear travelling wave motor,” Master’s thesis, Massachusetts Institute of Technology, 1990.
[9] W. Seemann, “A linear ultrasonic traveling wave motor of the ring type,” Smart materials and structures, vol. 5, no. 3, p. 361, 1996.
[10] M. Hermann and W. Schinköthe, “Piezoelectric travelling wave motors generating direct linear motion,” in Conference Proceedings, S, vol. 200, 1999, p. 203.
[11] J. Gere and S. Timoshenko, “Mechanics of materials.” Cole, Pacific Grove, CA, USA, 2000.
[12] S. P. Timoshenko, “Résistance des matériaux,” Paris: Dunod, c1968/1972, vol. 1, 1968.

Xinchang Liu was born in Beijing, China, in 1987. He received both a M. Sc. degree in electrical engineering from Beihang University in China and a M. Sc. degree in system and control from SUPÉLEC in France in 2012. He is currently PhD student in the Integrated Actuator Laboratory at EPFL. His research interests are design of piezoelectric actuators and its application.

Yoan Civet graduated from Grenoble Institute of Technology in France, Swiss Federal Institute of Technology - Lausanne (EPFL) in Switzerland and Politechnico di Torino in Italy (M. Sc. in Micro and Nanotechnologies for Integrated Systems) in 2008, received the PhD degree in Nanoelectronics and Nanotechnologies from the Université de Grenoble, France, in 2012 for his thesis on MEMS resonators. He then worked on piezoelectric MEMS resonator for haptic devices at TIMA laboratory, Grenoble, France. In 2013, he joined EPFL as Postdoctoral Fellowship. His research activities involve piezoelectric actuators, MEMS, magnetic devices and power transfer.

Yves Perriard was born in Lausanne in 1965. He received the M. Sc. in Microengineering from the Swiss Federal Institute of Technology - Lausanne (EPFL) in 1989 and the PhD. degree in 1992. Senior lecturer from 1998 and professor since 2003, he is currently director of the Integrated Actuator Laboratory at EPFL. His research interests are in the field of new actuator design and associated electronic devices.